Current Research in Pharmacology and Drug Discovery 4 (2023) 100148

Contents lists available at ScienceDirect

Current Research in Pharmacology and Drug Discovery

journal homepage: www.journals.elsevier.com/current-research-in-pharmacology-and-drug-discovery

A new triphenylphosphonium-conjugated amphipathic cationic peptide with improved cell-penetrating and ROS-targeting properties

Rezeda A. Ishkaeva [a], Diana V. Salakhieva [a], Ruslan Garifullin [a,b], Raghad Alshadidi [a], Alexander V. Laikov [a], Abdulla A. Yergeshov [a], Marat I. Kamalov [a], Timur I. Abdullin [a,*]

[a] Department of Biochemistry, Biotechnology, Pharmacology, Institute of Fundamental Medicine and Biology, Kazan Volga Region Federal University, 18 Kremlyovskaya St., 420008, Kazan, Russia

[b] Department of Aeronautical Engineering, University of Turkish Aeronautical Association, Türkkuşu Kampüsü, 06790, Ankara, Turkey

ARTICLE INFO

Keywords:
Amphipathic cationic peptides
Triphenylphosphonium cation
Intramolecular interaction
Cellular pharmacokinetics
Redox activity
ROS targeting

ABSTRACT

We study for the first time whether triphenylphosphonium (TPP) moiety can improve cellular delivery and redox properties of amphipathic cationic peptides based on YRFK/YrFK cell-penetrating and cytoprotective motif. TPP moiety was found to increase reducing activity of both stereoisomeric peptides in solution and on electrode surface in association with TPP-mediated intramolecular interactions. Among TPP-conjugated peptides, newly synthesized TPP3-YrFK featured both increased antioxidant efficacy and proteolytic resistance. TPP-conjugated peptides preferably mitigated endogenic ROS in mitochondria and cytoplasm of model glioblastoma cells with increased oxidative status. This anti-ROS effect was accompanied by mild reversible decrease of reduced glutathione level in the cells with relatively weak change in glutathione redox forms ratio. Such low interference with cell redox status is in accordance with non-cytotoxic nature of the compounds. Intracellular concentrations of label-free peptides were analyzed by LC–MS/MS, which showed substantial TPP-promoted penetration of YrFK motif across cell plasma membrane. However, according to $\Delta\Psi_m$ analysis, TPP moiety did not profoundly enhance peptide interaction with mitochondrial inner membrane. Our study clarifies the role of TPP moiety in cellular delivery of amphipathic cationic oligopeptides. The results suggest TPP moiety as a multi-functional modifier for the oligopeptides which is capable of improving cellular pharmacokinetics and antioxidant activity as well as targeting increased ROS levels. The results encourage further investigation of TPP3-YrFK as a peptide antioxidant with multiple benefits.

1. Introduction

Solid-phase peptide synthesis (SPPS) is an established powerful technique to develop and produce peptide sequences for therapeutic and diagnostic applications (Chan and White, 1999). In comparison with recombinant protein production, SPPS is generally restricted by shorter peptides with less than 50 amino acid (aa) residues, nevertheless it provides much greater possibilities for *in situ* modification of biomimetic peptides with both natural (aa isomers, saccharides, lipids) and non-natural synthetic moieties. Conjugation with the synthetic moieties is a promising strategy to generate hybrid peptides with improved physicochemical, pharmacokinetic, and pharmacological properties. The latter strategy is particularly aimed at overcoming rapid biodegradation of the therapeutic peptides and their poor accumulation in targeted cells (Yang et al., 2021; Lucana et al., 2021; Gentilucci et al., 2010).

Among pharmacologically relevant synthetic moieties, delocalized

Abbreviations: aa, amino acid; ABTS, 2,2′-azino-bis(3-ethylbenzthiazoline-6-sulfonic acid); CD, circular dichroism; CCCP, carbonyl cyanide 3-chlorophenylhydrazone; DCFDA, 2′,7′-dichlorofluorescin diacetate; GSH, reduced glutathione; HBSS, Hank's balanced salt solution; LC–MS/MS, liquid chromatography tandem mass-spectrometry; MRM, multiple reaction monitoring; MCB, monochlorobimane; ROS, reactive oxygen species; SPPS, solid-phase peptide synthesis; TPP, triphenylphosphonium.

* Corresponding author. Department of Biochemistry, Biotechnology and Pharmacology, Institute of Fundamental Medicine and Biology, Kazan Federal University, 18 Kremlyovskaya St., 420008, Kazan, Russia.

E-mail addresses: rezaahmadishina@kpfu.ru (R.A. Ishkaeva), divsalahieva@kpfu.ru (D.V. Salakhieva), chemist84@gmail.com (R. Garifullin), ra-alshadidi@stud.kpfu.ru (R. Alshadidi), avlajkov@kpfu.ru (A.V. Laikov), abdulla.ergeshov@mail.ru (A.A. Yergeshov), mikamalov@kpfu.ru (M.I. Kamalov), timur.abdullin@kpfu.ru (T.I. Abdullin).

https://doi.org/10.1016/j.crphar.2022.100148
Received 17 June 2022; Received in revised form 14 November 2022; Accepted 14 December 2022

lipophilic cations such as triphenylphosphonium (TPP) compounds have proved to be a powerful modifier for existing drugs. TPP modifiers, which are generally considered biochemically inert, act by driving a conjugated cargo into living cells and mitochondria by the electrochemical gradient across the plasma and mitochondrial membranes (Zielonka et al., 2017). To date, numerous low molecular weight drug molecules were successfully modified with TPP cation, resulting in improved drug candidates for treating cancer (Tsepaeva et al., 2017, 2020, 2021; Theodossiou et al., 2013), infectious (Tsepaeva et al., 2020; Nazarov et al., 2017; Wang et al., 2021), and degenerative diseases (Wang et al., 2020).

In spite of enormous interest in using TPP carriers, few works have been devoted to TPP-conjugated therapeutic peptides. FFK peptide coupled with 6-(triphenylphosphonio)hexyl via ε-amino group of lysine was synthesized as a cancer cell-damaging agent. The compound accumulated in mitochondria and formed stiff mitochondria-damaging fibrils as a result of diphenylalanine self-assembly (Kim et al., 2020; Hong et al., 2021). Similarly, single or multiple 5-(triphenylphosphonio)pentanoyl moieties were linked to D-$(KLAKLAK)_2$ proapoptotic peptide via ε-amine(s) of Lys_n-Ahx- linker ($n = 1–3$) (Kolevzon et al., 2011). Three TPP moieties were required to render these conjugates active against cancer cells (Kolevzon et al., 2011), reflecting poor translocating ability of peptide molecules across lipid membranes (Yang and Hinner, 2015). Furthermore, no promoting effect on cellular and mitochondrial uptake of cell-penetrating peptides Tat (YGRKKRRQRRRP) and penetratin (RQIKIWFQNRRMKWKK) was reported after N-terminal coupling with a single TPP group irrespective of alkyl linker length (C_4, C_8, C_{12}) (Ross et al., 2004; Ross and Murphy, 2004).

In contrast to the aforementioned peptides, the conjugates of model hemagglutinin A epitope YPYDVPDYA with 5-(triphenylphosphonio) pentanoic acid (via Lys_n-Ahx- linker) exhibited increased cellular and mitochondrial accumulation in proportion to the number of carrier groups ($n = 1–3$) (Abu-Gosh et al., 2009). Notably, these peptide-TPP conjugates were labelled with relatively bulky fluorophore molecules (FITC, Cy5, Oregon Green), though even smaller dansyl group was shown to profoundly change cellular pharmacokinetics of oligopeptides (Szeto et al., 2005). Carrier activity of the TPP moiety toward peptide-like cargo such as cell-impermeant iron chelator desferrioxamine (Alta et al., 2017) and poly(amidoamine) dendrimer (PAMAM, 4 generation) (Bielski et al., 2015) was also reported. Multiple-modified PAMAM showed increased cellular internalization and mitochondrial targeting (ca. 5 TPP groups) as well as enhanced cytotoxicity (ca. 10 TPP groups), which were decreased by introducing polyethylene glycol (PEG) linker between the moieties (Bielski et al., 2015). In addition to the above drug-related applications, TPP-conjugated cyclo-RGD peptide was proposed as a cellular modulator, which induces the formation of multicellular tumor spheroids in culture (Akasov et al., 2016).

The existing data do not clearly reveal the potential of TPP modifiers in developing therapeutic peptides. Along with improving bioavailability, an important unaddressed issue is whether the TPP moiety can modulate specific activities of the peptide molecules. The modulation of small bioactive peptides is envisaged, for instance, via induction of physicochemical and conformational changes in the peptide moiety by the TPP cation. The promising structures to be evolved using the TPP modifier are amphipathic cationic tetrapeptides composed of alternating aromatic and cationic amino acids, which have been recognized as cell-penetrating, mitochondria-modulating and cytoprotective compounds (Szeto, 2008; Sheu et al., 2006; Rocha et al., 2010).

In particular, Szeto-Schiller (SS) tetrapeptides were earlier discovered as biomimetic peptide agonists of μ-opioid receptors and cellular antioxidants with their active sequences generally evolved as follows: Tyr--^{D}Arg-Phe-Lys-NH_2 (SS-01), Dmt-^{D}Arg-Phe-Lys-NH_2 (SS-02, Dmt – dimethyltyrosine), ^{D}Arg-Dmt-Lys-Phe-NH_2 (SS-31) (Szeto, 2008; Sheu et al., 2006; Rocha et al., 2010). These peptides rapidly penetrate plasma membrane escaping endocytic pathways; moreover, they accumulate at the inner mitochondrial membrane with low dependence on the mitochondrial potential and exert versatile cytoprotective and antiapoptotic effects mainly attributed to the scavenging of reactive oxygen species (ROS) generated by mitochondria (Szeto, 2008; Sheu et al., 2006; Rocha et al., 2010).

The therapeutic potential of SS-peptides was established using different *in vitro* and *in vivo* models of degeneration-related disorders of the cardiovascular system (Dai et al., 2011; Escribano-Lopez et al., 2018; Allen et al., 2020), central nervous system (Szeto, 2006a; Manczak et al., 2010; Toyama et al., 2018), lung (Powers et al., 2011), kidney (Mizuguchi et al., 2008) (see also reviews (Rocha et al., 2010; Toyama et al., 2018; Meloni et al., 2020)). Recently, additional mitoprotective mechanisms of SS-31 peptide were reported. These are based on its affinity binding to mitochondrial membrane cardiolipin to improve structural organization and bioenergetics of mitochondria under stress conditions (Allen et al., 2020; Toyama et al., 2018; Mitchell et al., 2020; Chavez et al., 2020).

With respect to SS-peptides, the TPP cation can be considered as a synthetic analog of both aromatic and cationic amino acids. We have previously shown that N-terminal conjugation of YRFK motif with TPP-carboxylic acid drastically alters spatial structure and some biointeractions of the peptides depending on the presence of L- or D-isomer of arginine and the length of alkylene linker in the TPP moiety (Akhmadishina et al., 2018; Garifullin et al., 2019). The TPP-conjugated peptides increased viability of mammalian cells subjected to acute damage by oxidative agents (Akhmadishina et al., 2018).

This study provides important findings on multiple effects of the TPP moiety on pharmacological properties of YRFK derivatives *in vitro*. In particular, it shows whether delivery of the motif can be promoted by the TPP moiety at cellular and mitochondrial levels, providing quantification of intracellular concentration of the conjugated peptides. Furthermore, the study proposes the TPP moiety as a redox modulator for the peptides, which can specifically enhance antioxidant efficacy of YRFK derivatives and their targeting ability toward endogenic cellular ROS. The study also identifies a new proteolytically stable and cell-penetrating TPP-conjugated peptide as a potential inhibitor of oxidative stress.

2. Materials and methods

2.1. Materials

Rink amide MBHA resin, Fmoc-Tyr(tBu)-OH, Fmoc-Arg(Pbf)-OH, Fmoc-D-Arg(Pbf)-OH, Fmoc-Phe-OH, Fmoc-Lys(Boc)-OH, (5-carboxypentyl)triphenylphosphonium bromide, (2-carboxyethyl)triphenylphosphonium bromide, 2-(1H-benzotriazol-1-yl)-1,1,3,3-tetramethyluronium hexafluorophosphate (HBTU), N,N-diisopropylethylamine (DIPEA), triisopropylsilane (TIPS), trifluoroacetic acid (TFA), N,N-dimethylformamide (DMF), dichloromethane (DCM) were purchased from Merck and Fisher Scientific.

Monochlorobimane, JC-1, MitoSOX Red, MitoTracker™ Red CM-H2Xros dyes were purchased from ThermoFisher Scientific. 2,2′-azinobis(3-ethylbenzthiazoline-6-sulfonic acid) diammonium salt (ABTS), 2′,7′-dichlorofluorescin diacetate (DCFDA), carbonyl cyanide 3-chlorophenylhydrazone (CCCP), antimycin A, Hoechst 33258 were purchased from Sigma-Aldrich. Milli-Q grade water (Milli-Q® Advantage A10, Merck Millipore) was used to prepare buffers and solutions. Cell culture media and reagents were purchased from Paneco (Russia). LC–MS-grade solvents (Acros Organics) were used for mass-spectrometric analysis.

2.2. Peptide synthesis

Synthesis and structure characterization of YRFK-NH_2, YrFK-NH_2, TPP3-YRFK-NH_2, TPP6-YRFK-NH_2, TPP6-YrFK-NH_2 peptides were performed previously (Akhmadishina et al., 2018). TPP3-YrFK-NH_2 peptide was additionally synthesized as C-terminal amide by Fmoc solid-phase peptide synthesis (SPPS) method. Briefly, Rink amide resin was swollen in DMF and deprotected using 20% (v/v) piperidine in DMF. Subsequent coupling and deprotection cycles were carried out using 2

equiv. of Fmoc-protected amino acids, 1.98 equiv. of HBTU and 3 equiv. DIPEA in DMF. The peptide was cleaved from the resin in cleavage mixture (95% TFA, 2.5% H_2O, 2.5% TIPS), and collected with DCM, which was removed alongside with TFA on a rotary evaporator. Following trituration with cold diethyl ether, peptide was separated through centrifugation, and finally lyophilized.

2.3. Characterization of peptides

The synthesized peptides were purified by preparative HPLC and analyzed by LC–MS technique using the Agilent 1200/6530 instrument (Fig. S1).

The peptides were dissolved in phosphate-buffered saline (PBS, pH = 7) at a concentration of 400 μM. Circular dichroism (CD) spectra of the peptides were recorded on the Jasco J-1500 circular dichroism spectrophotometer in the wavelength region 250–300 nm. The CD measurements were performed in a 1 cm quartz cuvette with 6 accumulations. Fluorescence spectra of the peptides were recorded on the Horiba Jobin Yvon spectrofluorometer FL3-221-NIR using a 1 cm quartz cuvette at λ_{ex} = 275 nm (slit: 5 nm).

2.4. ABTS-radical scavenging assay

The ABTS microplate assay was performed according to the previous procedure (Ishkaeva et al., 2021) with some modifications. The scavenging activity was assessed in mixed methanol-water solution at final concentrations of the antioxidants of 0.2, 1, and 5 mM and ABTS of 0.4 mM. The reactive mixture was incubated for 10 min at room temperature followed by the detection of the optical absorbance at 734 nm on the Tecan Infinite M200PRO microplate analyzer.

2.5. Electrochemical analysis

The electrochemical analysis of the peptides on graphene oxide-modified electrodes (GOE) was performed as detailed previously (Ishkaeva et al., 2021). Briefly, 5 μL aliquot of 1 mM peptide aqueous solution was pre-incubated on the surface of GOE for 5 min and then rinsed with water. The adsorbed peptide molecules were detected using the square-wave voltammetry technique in the range of potentials 0–1.1 V at a frequency of 10 Hz, amplitude of 10 mV, and a potential step of 5 mV. The measurements were performed on the PalmSens EmStat potentiostat. The voltammograms were treated with PSTrace 5.5 software (Analytical mode).

2.6. Cell culture and viability

SNB-19 and LN-229 human glioblastoma cell lines (ATTC) as well as human skin fibroblasts (HSF) isolated from healthy donor (Tsepaeva et al., 2017) were used. The cells were cultured aseptically in DMEM containing 5% fetal bovine serum (FBS) for glioblastoma cells and in α-MEM containing 10% FBS for HSF, 2 mM L-glutamine, 100 U/mL penicillin and 100 μg/mL streptomycin at 37 °C in humidified air atmosphere with 5% CO_2. The MTT microplate proliferation assay (Akhmadishina et al., 2018) was performed after culturing the cells in the presence of peptides (0.04, 0.2 or 1 mM) for 24 h. Cell viability was presented relatively to the untreated cells (100% viability) as mean ± standard error (n = 3).

2.7. JC-1 and monochlorobimane (MCB) based microplate assays

Transmembrane potential of mitochondria in SNB-19 and LN-229 cells was assessed with JC-1 fluorescent probe. The cells were seeded in a 96-well plate and cultured until 80-90% cell confluency was reached. Then the cells were washed with Hank's balanced salt solution (HBSS), pre-stained with 2.5 μM JC-1 for 15 min and exposed to the peptides (0.04, 0.2, 1 mM) or CCCP (10 μM) for 2 h. The green fluorescence ($\lambda_{ex/em}$ = 490/530 nm) and red fluorescence ($\lambda_{ex/em}$ = 525/590 nm) were collected from the treated cells on the Infinite M200PRO analyzer, and the signal was presented as red to green fluorescence ratio (mean ± standard error, n = 4).

MCB–assisted detection of reduced glutathione (GSH) in living cells was performed as detailed in (Ishkaeva et al., 2022). The cells were seeded in a 96-well plate at a density of 20 × 10^3 cells per well in the culture medium and grown overnight. Next day, the cells were exposed to the peptides for 2 h in HBSS followed by staining with 5 μM MCB for 1 h (both steps in CO_2-incubator). The relative increment of MCB fluorescence ($\lambda_{ex/em}$ = 380/480 nm) in the cells was detected as a measure of cellular GSH (Ishkaeva et al., 2022). The data were presented as mean ± standard error (n = 6).

2.8. DCFDA and MitoSOX based flow cytometry analysis

SNB-19 and LN-229 cells were collected by trypsinization, washed with HBSS and suspended in HBSS at a density of 1 × 10^6 cells/mL. The cells were exposed to the peptides in HBSS (0.2 or 1 mM) for 2 h. The treated cells were stained with 5 μM MitoSOX or 20 μM DCFDA for 20 min at 37°C to detect mitochondrial and cytoplasmic ROS, respectively. The analysis was performed on a Guava EasyCyte 8HT flow cytometer (Millipore, MA, USA) in the green (DCFDA) or red (MitoSOX) fluorescence regions.

2.9. Laser scanning confocal microscopy (LSCM)

SNB-19 and LN-229 cells were grown overnight in a 6-well plate on coverslips (diameter = 25 mm) at a density of 20 × 10^3 cells per coverslip. The cells were treated with 0.04 mM peptide solutions in HBSS for 2 h and then stained with 100 nM MitoTracker™ Red CM-H_2Xros and 3 μg/mL Hoechst 33258 for 40 min. LSCM analysis of the stained cells was performed in an Attofluor™ cell chamber (ThermoFisher Scientific) and using the Zeiss LSM 780 confocal microscope with 63 × /NA 1.4 oil DIC M27 objective.

LSCM main parameters were as follows: dimensions x: 2048, y: 2048, 2 channels: 8-bit; master gain: 808; filter: 582-704; laser 543 nm: 89.7%. The mean fluorescence signals of the mitochondria in the control and treated cells were randomly collected from LSCM images (≥10 images) using a NIH ImageJ 1.48v software.

2.10. Liquid chromatography–tandem mass spectrometry (LC–MS/MS) analysis

2.10.1. GSH/GSSG ratio in peptide-treated cells

LC–MS/MS analysis in multiple reaction monitoring (MRM) mode was performed to quantify GSH and GSSG in the cells. The analysis was performed using an Infinity 1290 HPLC system (Agilent, Santa Clara, CA, USA) combined with a QTRAP 6500 triple quadrupole mass spectrometer (ABSciex, Singapore) equipped with Turbo Spray Ion Drive as an electrospray ionization (ESI) source. The parameters of chromatographic separation, generation of negatively charged ions and MRM transitions for GSH and GSSG were detailed previously (Ishkaeva et al., 2022).

The cells were seeded in 6-well plates (3.5 × 10^5 cells per well), precultured for 24 h and treated with 0.2 mM peptide solutions in HBSS for 5 h. Then the cells were scraped and lysed with 1% TFA solution on ice for 10 min. The cell lysates were frozen at −80 °C, thawed and diluted with mQ water to obtain final cell density of 1 × 10^6 cells/mL and TFA concentration of 0.1%. GSH and GSSG standards in TFA solution were used.

2.10.2. Proteolytic cleavage and cellular accumulation of peptides

The source parameters used in the study were as follows: capillary voltage 5.2 kV, gas 1 pressure 60 psi, gas 2 pressure 60 psi, curtain gas pressure 35 psi, temperature 500 °C. The quantifier/qualifier ions m/z, declustering potential, and collision energy were optimized for each

analyte using an automated "Compound optimization" algorithm of the Analyst 1.6.2 software (ABSciex, MA, USA).

The transitions monitored were: TPP3-YrFK (*m/z* 310.3 → 318.6 and *m/z* 310.3 → 452.2), YrFK (*m/z* 306.7 → 129.0 and *m/z* 306.7 → 320.0), TPP6-YrFK (*m/z* 324.2 → 339.6 and *m/z* 324.2 → 129.1). Compounds were separated on a Discovery HS C18 column (3 μm, 5 cm × 2.1 mm, Supelco, Sigma-Aldrich, USA) with mobile phases consisting of A (99.9% water, 0.1% formic acid) and B (94.9% acetonitrile, 5% water, 0.1% formic acid). The flow rate was 0.4 ml/min throughout the following 5 min multistep gradient (min – % phase B): 0–0.1 min – 1%, 0.1–2.6 min – up to 40%, 2.6–2.7 min – up to 95%, 2.7–3.7 min – 95%, 3.7–3.8 min – decrease to 1%, 3.8–5.0 min – 1%. All reagents used for the MS analysis were of LC–MS grade (Sigma Aldrich).

For studying proteolytic stability, YrFK and TPP3-YrFK (1 μM) were mixed with trypsin (0.02 μg/mL) in 50 mM Tris-HCl (pH = 7.4), and the mixture was incubated at room temperature. The concentration of undigested peptides was quantified over time.

For studying cellular penetration, SNB-19 cells suspended in HBSS (1×10^6 cells in 1 mL) were incubated with YrFK, TPP3-YrFK or TPP6-YrFK (0.2 mM) for 2 h upon gentle agitation in CO_2-incubator. The treated cells were washed with PBS, pelleted by centrifugation and frozen in low-temperature freezer. The cell pellet was mixed with methanol-water mixture (200 μL) in ice bath for lysis followed by the centrifugation of cell debris. The supernatant was analyzed using the above LC–MS/MS procedure.

2.11. Statistical analysis

Data were presented as mean ± standard error ($n = 3$), unless otherwise stated. Statistical significance was determined by two-way analysis of variance (ANOVA) followed by Bonferroni post-test to compare replicate means by row ($^*p < 0.05$, $^{**}p < 0.01$, $^{***}p < 0.001$).

3. Results

3.1. TPP moiety promotes antioxidant activity of conjugated peptides depending on intramolecular association

Six peptides based on YRFK biomimetic sequence were synthesized (Fig. 1), including previously characterized structures YRFK, YrFK, TPP3-YRFK, TPP6-YRFK, TPP6-YrFK (Akhmadishina et al., 2018) and a new TPP-conjugated peptide TPP3-YrFK. In the above abbreviations, R/r are L-/D-Arg residues and TPP3/TPP6 are TPP-propanoyl/TPP-hexanoyl groups; C-amide group is omitted for simplicity. Radical-scavenging properties of the compounds were assessed by the ABTS assay with increased sensitivity compared to the DPPH assay (Ishkaeva et al., 2021). The unmodified peptides YRFK and YrFK did not scavenge ABTS radical under assay conditions; their conjugates with the TPP6 group possessed a significant but relatively weak scavenging effect (Fig. 2A).

TPP3-YRFK and TPP3-YrFK similarly to each other showed superior ABTS scavenging in proportion to the concentration (Fig. 2A). The enhanced antiradical activity of the TPP3-derived conjugates can be explained through their distinctive spatial structure, which features intramolecular association of the TPP cation with side aromatic groups of Tyr and Phe residues according to previous comparative analysis of TPP3-YRFK and TPP6-YRFK using NMR and circular dichroism (CD) spectroscopy (Garifullin et al., 2019). Similarly, CD spectrum of TPP3-YrFK contained a characteristic induction signal in the wavelength range 250–300 nm, which was not observed for TPP6-YrFK (Fig. 3A), indicating specific aromatic-aromatic interactions in the TPP3-conjugated peptide.

In addition, fluorescence spectroscopy revealed a considerable decrease of Tyr emission intensity in TPP3-YrFK compared to YrFK and TPP6-YrFK (Fig. 3B) attributed to quenching of Tyr fluorescence due to TPP3-mediated π-π intrapeptide interactions. Together, these data suggest that the TPP3 group with a shorter linker modulates Tyr characteristics in both YrFK and YRFK in a specific way, promoting radical-quenching activity of Tyr considered as a redox center (Nag et al., 2017).

To further assess the redox-modulating effect of the TPP moiety, the peptides were subjected to voltammetric analysis using graphene oxide-modified electrodes with increased sensitivity (Ishkaeva et al., 2021). After pre-incubation on the electrode surface, the peptides generated well-defined symmetrical peaks in the anodic region (Fig. 2B), indicating both effective adsorption and oxidation processes.

Among the compounds, TPP3-YRFK and TPP3-YrFK exhibited significantly lower oxidation potential (E_{ox}) (Fig. 2B and C) and thus better electron-donating ability of Tyr. The detected effect of the TPP3 group on E_{ox} was still low (compared to ABTS-quenching effect), seemingly due to its underestimation as a result of disruption of intramolecular aromatic association of the conjugates by graphene structures (Zhang et al., 2013). In its turn, the intramolecular association is expected to competitively decrease hydrophobic adsorption and detection of the conjugates on the modified electrode. This is supported by significantly lower currents of TPP3-YRFK and TPP3-YrFK compared to TPP6-YRFK and TPP6-YrFK counterparts pre-adsorbed on the electrode (Fig. 2B and C).

All the synthesized peptides did not decrease viability of mammalian cells at a concentration as high as 1 mM as demonstrated using both primary human skin fibroblasts and glioblastoma cells (Fig. S2). To further assess antioxidant properties of the compounds, SNB-19 and LN-

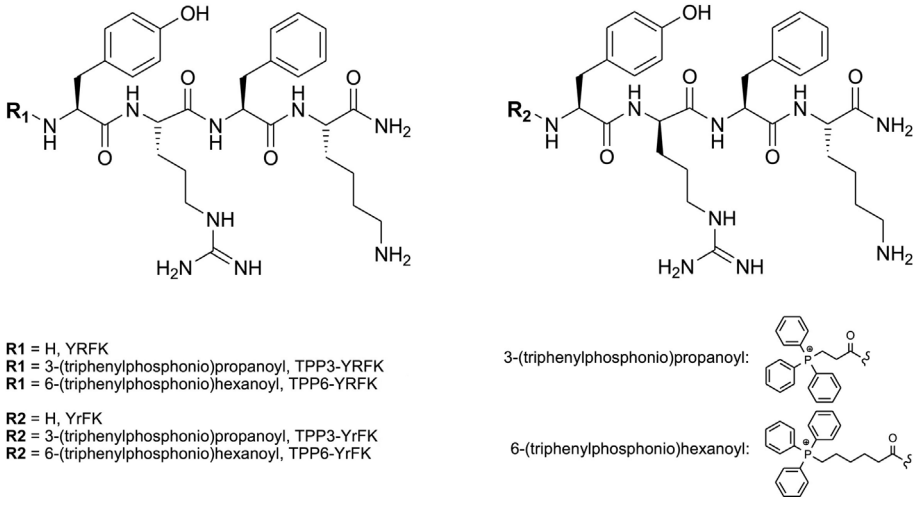

Fig. 1. Structural formulas of YRFK motif-based peptides and their TPP derivatives.

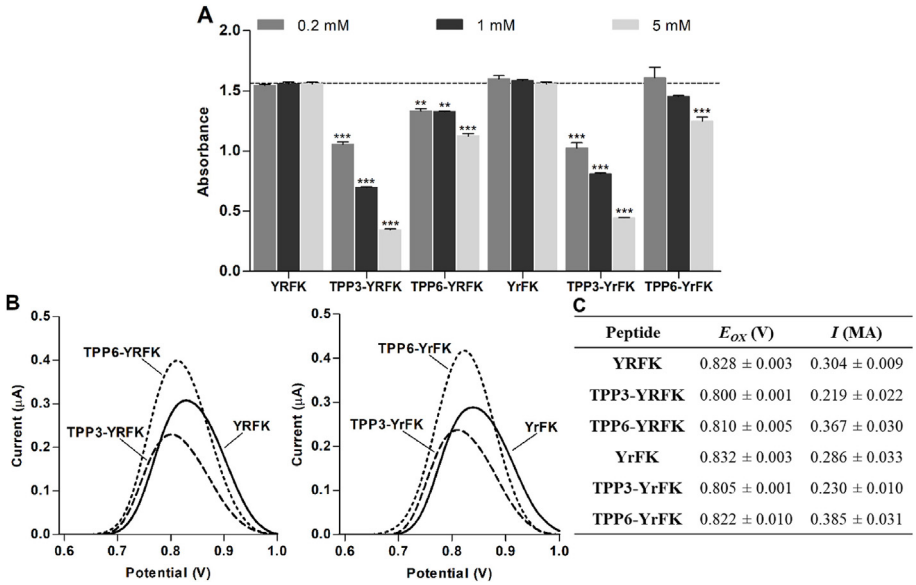

Fig. 2. Antioxidant properties of TPP-conjugated peptides. (A) ABTS radical-scavenging activity in solution. (B) Square-wave voltammograms of peptides adsorbed and oxidized on graphene oxide-modified electrode. (C) Mean values of oxidation potential (E_{ox}) and oxidation current (i) of electrochemically detected peptides. Mean ± SEM ($n = 3$, $^{**}p < 0.01$, $^{***}p < 0.001$ vs. Ctrl) are shown for A.

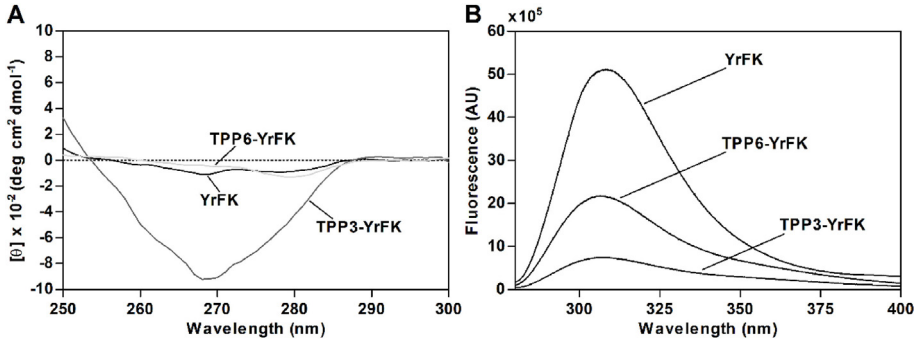

Fig. 3. (A) Representative circular dichroism and (B) fluorescence emission spectra of YrFK, TPP3-YrFK and TPP6-YrFK (0.4 mM) in PBS. For (B) $\lambda_{ex} = 275$ nm was used.

229 human glioblastoma cells were employed as model pre-characterized cells with distinctly different levels of cytoplasmic and mitochondrial ROS (Ishkaeva et al., 2022). Cellular effects of the TPP-conjugated peptides were studied and compared at non-cytotoxic (sub)millimolar concentrations.

3.2. TPP-conjugated peptides do not dissipate mitochondrial potential

The effect of compounds on transmembrane potential of mitochondria ($\Delta\Psi_m$) in the glioblastoma cells was initially assessed since the dissipation of $\Delta\Psi_m$ contributes to mitocondrial ROS production (Huang et al., 2008) and also characterizes mitochondria-penetrating activity (Horton et al., 2008, 2012). Two-hour cell exposure to the peptides (0.04, 0.2, 1 mM) caused concentration-sensitive modulation of $\Delta\Psi_m$ according to JC-1 fluorescence (Fig. 4). YrFK in contrast to YRFK noticeably increased $\Delta\Psi_m$ by up to ca. 40%. Such a hyperpolarizing activity could be associated with electrostatic binbding of the peptide to the mitochondrial inner membrane (MIM) without internalization into the matrix (Szeto, 2006a, 2006b). It is seemingly favored by relative proteolytic stability of YrFK rendered by D-Arg residue (Szeto, 2006a, 2006b; Akhmadishina

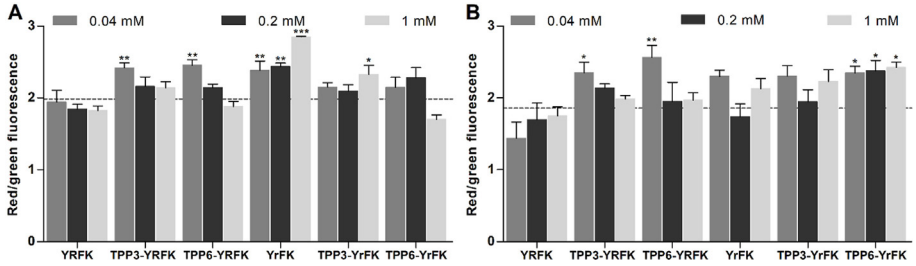

Fig. 4. Effect of TPP-conjugated peptides on transmembrane potential of mitochondria in (A) SNB-19 and (B) LN-229 glioblastoma cells after 2-h treatment according to JC-1 fluorescence. Mean ± SEM ($n = 4$, $^{*}p < 0.05$, $^{**}p < 0.01$, $^{***}p < 0.001$ vs. Ctrl) are shown. Dotted line shows the signal for untreated cells.

et al., 2018) to increase half-life and mitochondrial concentration of the peptide.

The TPP-conjugated peptides were generally characterized by different increasing effects on $\Delta\Psi_m$. For instance, TPP3-YRFK and TPP6-YRFK significantly increased $\Delta\Psi_m$ mainly at a lower concentration of 0.04 mM, whereas TPP3-YrFK and TPP6-YrFK showed more variable concentration-dependent effects (Fig. 4). Such a mitochondrial hyperpolalization presumably occurs at certain concentrations of the peptides at MIM. The TPP moiety is expected to increase mitochondrial accumulation of the conjugated peptides by $\Delta\Psi_m$-driven transportation and modulation of proteolytic resistance. The results demonstrate that the TPP-conjugated peptides do not induce mitochondria depolarization in contrast to more lipophilic non-peptide TPP derivatives (Tsepaeva et al., 2017, 2020, 2021).

3.3. TPP-conjugated peptides preferably inhibit increased cellular ROS levels

3.3.1. Effect on cytoplasmic ROS

As previously shown, LN-229 cells were characterized by increased oxidative status and decreased content of reduced glutathione (GSH) in comparison with SNB-19 cells (Ishkaeva et al., 2022). According to DCFDA fluorescence, both LN-229 and SNB-19 cells contained two populations denoted as 1 and 2 with higher and lower cytoplasmic ROS level, respectively (Fig. 5). The antioxidant activity of the peptides was manifested by the reduction of cell number in the population 1 and its concomitant increase in the population 2, indicating preferable effect on the cells with overproduced ROS. Such an effect was much more pronounced in LN-229 cells. For the YRFK derivatives it increased as follows: YRFK < TPP3-YRFK ≤ TPP6-YRFK with a similar relationship for the YrFK derivatives. The latter compounds, however, exhibited enhanced antioxidant activity so that they decreased the population 1 by up to ca. 50% (0.2 mM) and 70% (1 mM) (Fig. 5).

3.3.2. Effect on mitochondrial ROS

The level of mitochondrial ROS was assessed by cytofluorimetry with MitoSOX as a conventional mitochondria-targeted probe for superoxide radical (Fisher Scientific, 2017). The compounds decreased mitochondrial ROS in treated SNB-19 cells by averagely 21%; more pronounced ROS inhibition was induced in LN-229 cells in the following order: YRFK < YrFK < TPP conjugates. The most active conjugates TPP3-YrFK and TPP6-YrFK (0.2 mM) caused as high as 3-fold decrease in the ROS level (Fig. 6).

Since MitoSOX fluorescence can be contributed by other intracellular structures beside mitochondria (Roelofs et al., 2015), mitochondrial ROS were additionally visualized by Mitotracker Red CM-H_2XRos using LSCM. Comparable $\Delta\Psi_m$ of the studied cells and the lack of depolarizing activity of the peptides allowed for using the latter probe regardless its $\Delta\Psi_m$-dependent accumulation in mitochondria (Fisher Scientific, 2017). The microscopy analysis confirmed that LN-229 cells featured considerably higher mitochondrial ROS level compared to SNB-19 cells (Fig. 7). Furthermore, it provided more sensitive detection of anti-ROS effect of the peptides, which clearly appeared at a concentration of 0.04 mM (on the example of YrFK derivatives). Among the compounds, TPP3-YrFK diminished ROS in LN-229 cells in a more effective way by ca. 3 times so that the ROS level similar to that in untreated SNB-19 cells was achieved (Fig. 7).

The results support that the TPP moiety substantially enhances antioxidant activity of YRFK/YrFK motif against both cytoplasmic (Fig. 5) and mitochondrial (Fig. 6) ROS. Different analyses (Figs. 2, 5–7) showed that the activity of TPP3-YrFK and TPP6-YrFK may somewhat differ toward each other presumably due the effect of assay conditions as well as depending on degradation rate of the conjugates (see Section 3.4.). Altogether, compared to the initial peptide motif, TPP3-YrFK and TPP6-YrFK can be identified as improved cellular antioxidants, which can target the cells with increased oxidative state, preferably inhibiting overproduced ROS levels.

3.3.3. Effect on cellular glutathione

In view of similar antioxidant activity of YRFK and YrFK derivatives (Fig. 2) and increased proteolytic stability of the latter compounds (Akhmadishina et al., 2018), the YrFK-derived conjugates were selected for further study. The relationship of their anti-ROS activity with the production of glutathione as a key cellular antioxidant was examined. According to monochlorobimane-based microplate assay in living cells (Ishkaeva et al., 2022), after 2-h exposure, the compounds moderately decreased the level of reduced glutathione (GSH) in both SNB-19 and LN-229 cells by up to 40% with somewhat higher effect of the

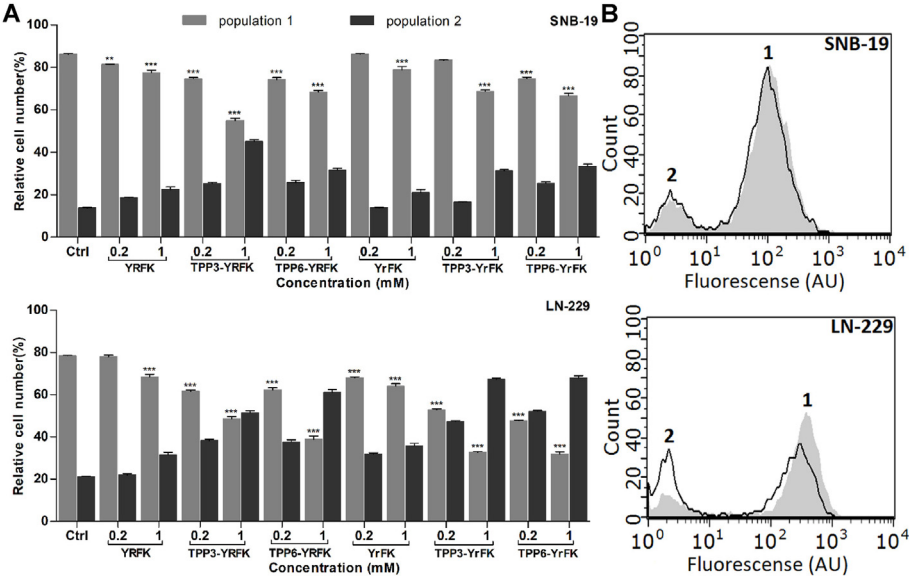

Fig. 5. Inhibition of endogenous cytoplasmic ROS in SNB-19 and LN-229 cells by TPP-conjugated peptides (2-h treatment) according to flow cytofluorometry with DCFDA probe. (A) Relative cell number (total amount = 100%) in cell populations 1 and 2. (B) Fluorescence distributions in control cells (filled curve) and cells treated with 0.2 mM TPP3-YrFK (unfilled curve). Mean ± SEM ($n = 3$, $^*p < 0.05$, $^{**}p < 0.01$, $^{***}p < 0.001$ vs. Ctrl).

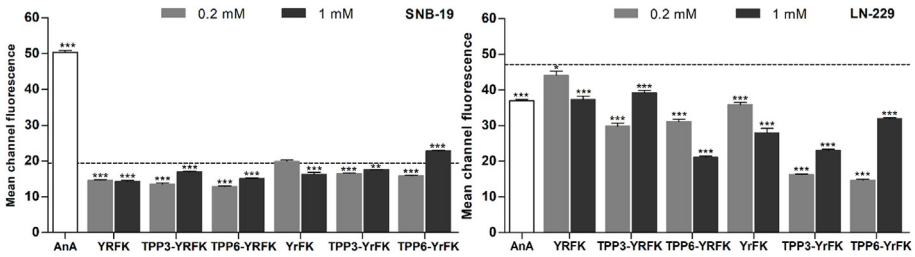

Fig. 6. Inhibition of endogenic mitochondrial ROS in SNB-19 and LN-229 cells by TPP-conjugated peptides (2-h treatment) according to flow cytofluorometry with MitoSOX probe. Mean channel fluorescence values ± SEM ($n = 3$, $^{*}p < 0.05$, $^{**}p < 0.01$, $^{***}p < 0.001$ vs. Ctrl) are shown. Dotted line shows the signal for untreated cells.

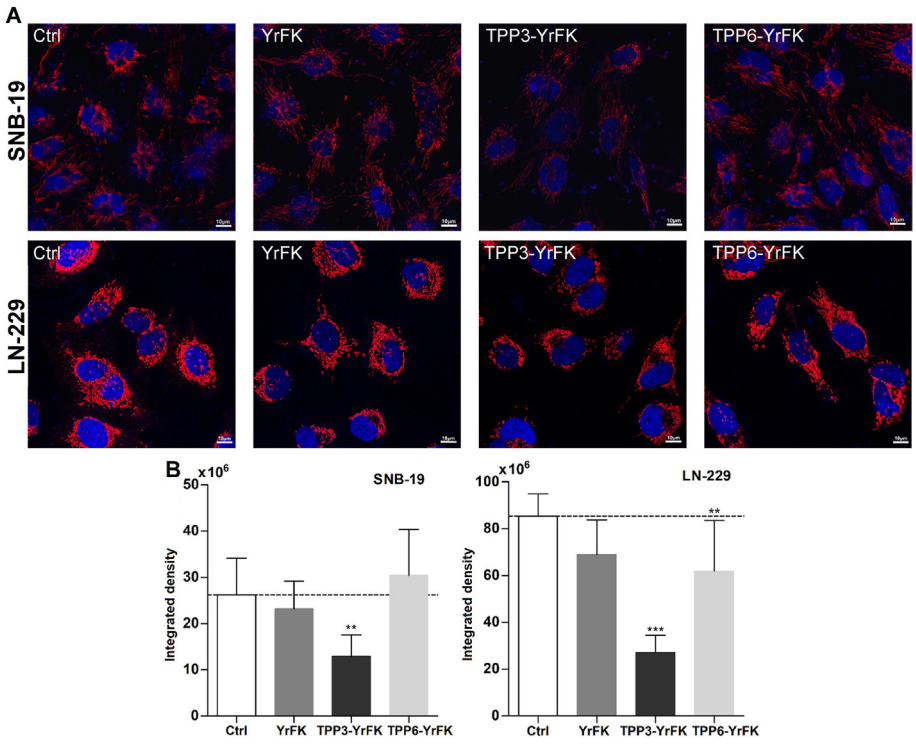

Fig. 7. (A) Typical LSCM images of SNB-19 and LN-229 cells treated with YrFK, TPP3-YrFK, TPP6-YrFK (40 μM, 2 h) and stained with Mitotracker Red CM-H_2XRos probe. (B) Relative density of mitochondria-associated fluorescence (red). Dotted line shows the signal for untreated cells. Mean ± SD ($n = 10$, $^{**}p < 0.01$, $^{***}p < 0.001$ vs. Ctrl) are shown. (For interpretation of the references to colour in this figure legend, the reader is referred to the Web version of this article.)

TPP-conjugated peptides (Fig. 8A).

After a more extended 5-h cell exposure to the peptides, the GSH pool was recovered (Fig. 8B), indicating cell adaptation to the antioxidant treatment and restoration of intrinsic GSH level. In addition, according to pre-optimized mass-spectrometric analysis of the ratio of GSH and oxidized glutathione (GSSG) (Ishkaeva et al., 2022), SNB-19 cells possessed higher ratio (Fig. 8C) contributed by a considerably increased content of reduced tripeptide in comparison with LN-229 cells (Table S1). 5-hour treatment of the both cells with the peptides was accompanied by similar moderate decrease of the ratio by 1.2–1.5 times mainly due to some increase in GSSG content. The detected GSH/GSSG ratios were far above critical values, which might trigger the apoptotic process (Aon et al., 2007). In LN-229 cells, TPP3-YrFK and TPP6-YrFK caused a weaker decreasing effect on the ratio than the unmodified peptide (Fig. 8C) due to decreased GSSG formation in the presence of the conjugates (Table S1). Altogether, the results support that profound anti-ROS activity of the TPP conjugates of YrFK is accompanied by a relatively weak alteration of cell redox status (see also Discussion section).

3.4. TPP moiety improves pharmacokinetics-related properties of YrFK motif

Enzymatic degradation and cellular penetration of TPP-conjugated YrFK were assessed using LC–MS/MS analysis. Fig. 9A shows optimized conditions for the detection of peptides by LC–MS/MS in MRM mode. Representative MS and MS/MS spectra and LC–MRM chromatograms of the peptides as well as corresponding calibration graphs are shown in Figs. S3 and S4.

Half-time of YrFK cleavage by trypsin was about 12 h (Fig. 9B), which was comparable to that observed under previous HPLC conditions (14 h) and much higher compared to YRFK (6 h) (Akhmadishina et al., 2018). For newly synthesized TPP3-YrFK, half-time digestion was 20 h, indicating ca. 1.7-fold higher proteolytic resistance of the conjugate compared to YrFK (Fig. 9B). This shows a significant inhibition of endopeptidase cleavage of YrFK motif by the TPP3 group, although TPP3-YrFK was found to be less resistant than TPP6-YrFK, which remained almost uncleaved by trypsin (Akhmadishina et al., 2018).

Table 1 summarizes found concentrations of the peptides in glioblastoma cells treated with the compounds. The results show that the TPP

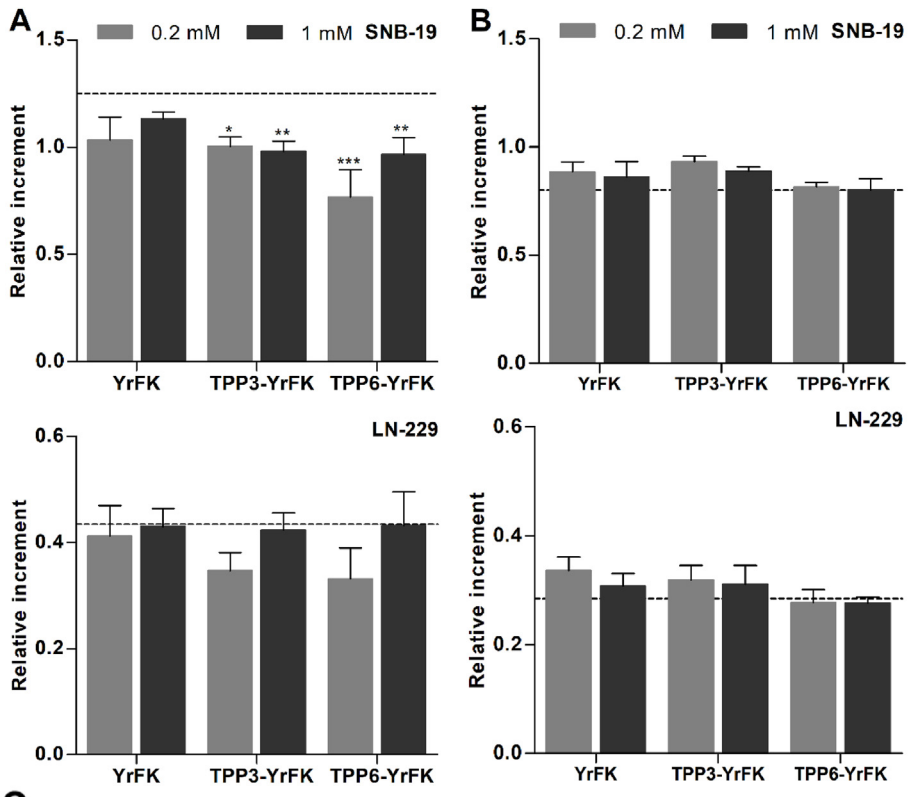

Fig. 8. Effect of TPP-conjugated YrFK on GSH content in SNB-19 and LN-229 cells after (A) 2-h and (B) 5-h treatment according MCB fluorescence (Ishkaeva et al., 2022). Dotted line shows the signal for untreated cells. (C) Effect of TPP-conjugated YrFK (0.2 mM) on GSH/GSSG ratio in the cells according to LC–MS/MS analysis. For (A) and (B) mean ± SEM ($n = 6$, $^{*}p < 0.05$, $^{**}p < 0.01$, $^{***}p < 0.001$ vs. Ctrl) are shown. For (C) the cells were treated for 5 h and lysed in TFA solution (1×10^6 cells in 1 mL); mean ± SD (from 3 biological and 3 technical repeats, $n = 9$, $^{**}p < 0.01$, $^{***}p < 0.001$ vs. Ctrl; $^{\#\#\#}p < 0.001$ vs. LN-229) are shown.

C

Samples	SNB-19	LN-229
Ctrl	192.5 ± 10.2 ###	136.7 ± 20.2
YrFK	137.1 ± 14.0 ***	94.0 ± 8.0 ***
TPP3-YrFK	149.1 ± 7.0 ***	105.8 ± 9.3 ***
TPP6-YrFK	141.1 ± 3.0 ***	114.2 ± 11.0 **

A

Peptide	Retention time, min	Q1, m/z	Q3, m/z	Declustering potential, V	Collision energy, V	Collision cell exit potential, V
YrFK	1.29	306.7	129.0*	31	21	10
			320.0	31	23	6
			84.0	31	47	8
TPP3-YrFK	2.27	310.3	318.6*	16	21	4
			452.1	16	33	8
			304.6	16	15	4
TPP6-YrFK	2.34	324.2	339.6*	36	21	4
			129.1	36	19	10
			120.1	36	25	10

*fragment used for quantitative analysis

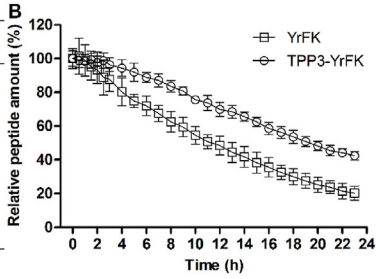

Fig. 9. (A) Optimized MRM parameters used for LC-MS/MS detection of YrFK, TPP3-YrFK and TPP6-YrFK. (B) Cleavage kinetics of YrFK and TPP3-YrFK (1 μM) by trypsin (0.02 μg/mL) in 50 mM Tris-HCl (pH = 7.4) according to LC-MS/MS.

moiety profoundly increases intracellular concentration of YrFK motif on average by 15 times (TPP3) and 10 times (TPP6), supporting better cellular availability of the TPP-conjugated peptides. By assuming average volume of a mammalian cell of 2000 μm^3, the intracellular concentration of TPP3-YrFK and TPP6-YrFK was estimated respectively as 61.7 and 41.1 μM vs. 4.1 μM for the unmodified peptide. Although longer aliphatic linkers commonly favor cellular availability of TPP-conjugated biomolecules (Zielonka et al., 2017; Tsepaeva et al., 2021), TPP3-YrFK exhibited better cellular delivery compared to TPP6-YrFK. This is explained by specific intramolecular association of TPP3-YrFK, which should provide a more compact spatial structure of the conjugate as earlier shown for TPP3-YRFK counterpart (Garifullin et al., 2019).

4. Discussion

Our study shows that both *in vitro* pharmacokinetic properties and

Table 1
Concentration (nM) of YrFK, TPP3-YrFK and TPP6-YrFK in lysates of SNB-19 cells (1×10^6 cells in 200 μL) incubated with 0.2 mM peptides for 2 h. Mean ± SD are shown ($n = 3$, $^{***}p < 0.001$ vs. YrFK; $^{\#}p < 0.05$, $^{\#\#\#}p < 0.001$ vs. TPP3-YrFK).

Sample No	YrFK	TPP3-YrFK	TPP6-YrFK
1	17 ± 0.1	392 ± 6.7***	232 ± 4***,###
2	73 ± 1.8	914 ± 2***	510 ± 2***,###
3	30 ± 0.2	544 ± 12***	490 ± 0.6***,###
Averaged data	**41 ± 26**	**617 ± 233*** **	**411 ± 135***,#**
Enhancement factor	—	**15**	**10**

Averaged data for three parallel samples (mean ± SD, $n = 3$); enhancement factor for TPP-mediated uptake.

specific antioxidant activity of amphipathic cationic peptides can be improved by conjugation with the TPP moiety. Although the TPP cation per se is not redox active, the TPP3 group with a shorter 3-carbon linker substantially increased radical-reducing ability of both YRFK and YrFK peptides, compared to the TPP6 group (Fig. 2A). Previous structural study (Garifullin et al., 2019) and the data for new TPP3-YrFK conjugate (Fig. 3) suggest that the TPP3 group provides a specific intramolecular association of the TPP cation and aromatic side-chain groups of both stereoisomeric peptides.

The resulting spatial structure of the TPP3-modified peptides favors π-π interactions of the phosphonium group with Tyr, seemingly leading to the formation of a transient charge transfer complex as supported by Tyr fluorescence quenching (Fig. 3B) and in accordance with reported electron-conducting properties of TPP-based ionic compounds (Prasad et al., 2020). The intramolecular TPP–Tyr association explains the facilitation of electron withdrawal from redox active Tyr hydroxyl as revealed by the ABTS assay as well as electrocatalyst-assisted voltammetry (Fig. 2). The latter analysis was employed as a useful technique to directly assess redox activity of peptide compounds, which nevertheless possess intrinsically poor electrochemical behavior compared to more lipophilic antioxidants (Ishkaeva et al., 2021).

Furthermore, ABTS-scavenging concentrations of the most reactive conjugates TPP3-YRFK and TPP3-YrFK were in submillimolar range (Fig. 2A), suggesting their inferior antioxidant power compared to Trolox and GSH with ca. 10 times lower effective concentrations (Ishkaeva et al., 2021). However, this did not compromise inhibitory activity of the conjugates against cellular ROS (Fig. 5–7). Moreover, it was hypothesized that such a moderate radical-scavenging activity of the TPP-conjugated peptides may provide better targeting of overproduced ROS levels. Such a specific action remains an important problem in antioxidant therapy of degenerative and cancer diseases, considering that highly reactive antioxidant compounds can disturb the redox homeostasis via different mechanisms, leading to controversial therapeutic outcomes (Forman and Zhang, 2021; Firuzi et al., 2011; Vassalle et al., 2020).

To verify the hypothesis, pre-characterized human glioblastoma cell lines SNB-19 and LN-229 were used, where the latter cells featured overproduced cytoplasmic and mitochondrial ROS, decreased thiol pool and higher responsiveness to supplemented thiols (Ishkaeva et al., 2022) (Fig. 5–8). The lack of ROS-promoting effect of antimycin A, the cytochrome *c* reductase inhibitor, in LN-229 cells (Fig. 6) may also indicate the role of mitochondrial dysfunction in increased oxidative status of the cells. Therefore, SNB-19 and LN-229 cells were regarded as related cells with different endogenous ROS levels, which could be useful to model sustained oxidative stress-related conditions.

The TPP-conjugated peptides displayed profoundly increased antioxidant activity *in vitro* over the unmodified peptides and, also importantly, were considerably more effective in decreasing ROS levels in LN-229 vs. SNB-19 cells and in cell population 1 vs. 2 (Figs. 5 and 6), thus preferably targeting the cells with increased ROS production. In particular, 0.2 mM TPP3-YrFK inhibited mitochondrial ROS by a factor of ca. 3 for LN-229 cells and only 1.2 for SNB-19 cells (Fig. 6). In more responsive LN-229 cells, the YrFK-derived conjugates showed significantly higher antioxidant effect compared to the YRFK-derived counterparts (Figs. 5 and 6). Taking into account similar radical-scavenging activity of these counterparts (Fig. 2), increased cellular activity of the YrFK-derived conjugates is explained by their higher proteolytic stability and half-life. These data allow to consider TPP3-YRFK and TPP3-YrFK as model stereoisomeric peptides with respectively fast and more prolonged antioxidant effects *in vitro*.

Summarizing the results (Fig. 5–7), the TPP-conjugated YrFK can be regarded as a cellular antioxidant against overproduced mitochondrial and cytoplasmic ROS. In this study, to compare cellular responses of the TPP conjugates and the unmodified peptides with quite different activities, the compounds were applied at submillimolar concentrations. Considering mitochondriotropic properties of both amphipathic cationic peptides and TPP compounds, the observed effects on mitochondrial ROS are expected to be saturated. Previously, cytoprotective effects of SS-31 peptide in the nanomolar range were reported (Zhao et al., 2005), although they were assessed under prolonged culture conditions and were not directly compared with anti-ROS activity. Direct inhibition of mitochondrial ROS by SS-31 peptide analogs was earlier detected at micromolar concentration after 24-h exposure (Cerrato et al., 2015). Due to the presence of highly reactive Dmt instead of Tyr, SS-31 peptide should be regarded as a strong antioxidant, which is presumably less capable of differentiating between ROS levels. The lack of standardized analyses for antioxidant peptides complicates a comparative assessment of the TPP-conjugated peptides with SS-31 peptide and related structures based on reported data. This task requires a separate study.

Among the SS-like structures, mtCPP-1, an improved SS-31 analog with lysine replaced by ornithine, was reported (Cerrato et al., 2015). Similarly, new amphipathic cationic peptides were synthesized including those containing tryptophan and proline residues. ^{D}Arg-Dmt-Arg--Phe-NH_2 (RF-2) peptide possessed comparable neuroprotective activity to that of SS-31 in zebrafish ototoxicity model, and both peptides when attached to poly (lactide-co-glycolide) nanoparticles similarly promoted their mitochondrial delivery (Sun et al., 2019).

An additional mechanism of cytoprotective activity of the SS-peptides, which does not rely on redox active Tyr/Dmt units, has been recently proposed. It involves a specific binding of the cationic peptides to highly anionic cardiolipin abundant in MIM (K_D is in the micromolar range). The bound peptides are capable of reducing surface charge of MIM without disturbing its lamellar structure while improving lipid packing (Mitchell et al., 2020). This effect allows to competitively inhibit excessive binding of calcium ions as well as mitotoxic basic proteins to MIM (Mitchell et al., 2020).

An important issue addressed in this study was whether the TPP moiety can promote the delivery of oligopeptide cargo into the cells and the mitochondrial matrix given that the existing data are controversial (Kim et al., 2020; Hong et al., 2021; Kolevzon et al., 2011; Ross et al., 2004; Ross and Murphy, 2004; Abu-Gosh et al., 2009; Szeto et al., 2005; Alta et al., 2017; Bielski et al., 2015). It should be noted that fluorescent labels often used to assess cellular pharmacokinetics of the amphipathic cationic peptides should alter their bioavailability (Zhao et al., 2003). Therefore, unlabeled YrFK, TPP3-YrFK and TPP6-YrFK were detected using pre-optimized LC–MS/MS procedure (Figs. S3 and S4). Direct evidence was obtained that the TPP3 and TPP6 groups up to 15 times promoted penetration of the conjugated peptide into mammalian cells (Table 1). The averaged intracellular concentration of the peptides was 36 μM, whereas extracellular one was 200 μM. This suggests effective translocation of the compounds across the plasma membrane similarly to that observed for the SS-peptides containing fluorescent analogs of aromatic amino acids (Zhao et al., 2003). Nevertheless, cellular uptake of the TPP-conjugated peptides seems to be inferior to that of more lipophilic TPP derivatives such as those of betulinic acid, which showed comparable accumulation in the cells at much lower extracellular concentration of 1 μM (unpublished data). Our results demonstrate that the TPP moiety allows to noticeably increase cellular availability of the conjugated YrFK in addition to augmenting its proteolytic stability (Table 1 and Fig. 9),

and both these factors should underlie improved pharmacokinetic properties of the compounds.

Regarding potential mitochondrial penetration, the TPP-conjugated peptides did not possess depolarizing and prooxidant activities in a wide concentration range. This indicates that the TPP moiety does not increase permeability of MIM as a result of its destabilization and/or penetration. Presumably, a single TPP cation does not provide sufficient electrochemically driving force for translocation of the peptides across MIM, even given their cell-penetrating and mitochondriotropic nature. Unlike the peptide compounds, the TPP conjugates of monocyclic biomolecules such as salicylic and acetylsalicylic acids had defined MIM-disturbing effects including $\Delta\Psi_m$ drop and mitochondrial ROS overoproduction accomponied by profound cytotoxicity, which was promoted by longer aliphatic linkers (Tsepaeva et al., 2021). Similar activities were observed for the TPP conjugates of polycyclic triterpenoids, excepting that these were not promoted or tended to decrease upon the linker extension (Tsepaeva et al., 2017), indicating the role of appropriate lipophilicity in mitochondrial delivery and toxicity of the TPP-modified cargo.

The relationships between physicochemical properties and cellular effects of amphipathic cationic oligopeptides were systematically studied in (Horton et al., 2008, 2012) using model structures containing Phe analog cyclohexylalanine (Fx) and D-arginine dipeptide repeats ($(F_Xr)_n$). Cellular uptake of these peptides was generally in proportion to their length (n = 2–6), whereas a critical length to induce mitochondria-disrupting and cytotoxic activities ($IC_{50} \leq 16$ μM) started from $n = 4$ (octapeptides) (Horton et al., 2012). Measured logP values for the structurally related peptides ($n = 4$, charge +5) varied between −2.2 and −2.7 (Horton et al., 2008).

The TPP conjugates of YRFK/YrFK obviously do not achieve a critical logP/cationic charge to induce mitochondrial penetration and toxicity. Mitochondriotropic properties of the TPP conjugates seem to differ quantitatively rather than qualitatively from those of the unmodified peptides, which were reported to concentrate at the MIM without penetration into the mitochondrial matrix (Szeto, 2008; Zhao et al., 2005; Cerrato et al., 2015). Even assuming that the TPP conjugates, similarly to the SS-peptides, accumulate in the intermembrane space of mitochondria, they effectively inhibit both mitochondrial and cytoplasmic ROS (Fig. 5–7).

The TPP-conjugated peptides did not show cytotoxicity toward primary HSF and glioblastoma cells (Fig. S2) in consistency with the lack of their mitochondria-disturbing effect. Furthermore, based on the analysis of cellular GSH and GSSG, the compounds did not induce marked change of cell redox status (Fig. 8). As previously reported, exogenic GSH strongly affected endogenic level of the tripeptide in mammalian cells, increasing the level in the cells with GSH deficiency and decreasing it in GSH-rich cells (Ishkaeva et al., 2022). Pharmacological increase of cellular GSH seems to be favorable upon GSH depletion, whereas overproduction of the tripeptide seems to readily disturb cell homeostasis and induce oxidative stress (Ishkaeva et al., 2022; Zhang et al., 2011). Trolox and N-acetylcysteine (NAC) were shown to elevate GSH/GSSG ratio in melanoma cells by ca. 2.5 and 3.8 times respectively, promoting metastatic ability of the cells (Le Gal et al., 2015). Both GSH and GSSG levels in V79 lung fibroblasts increased up to 2 times in the presence of NAC (Grosicka-Maciąg et al., 2011). Based on these data, the lack of increasing (or strong decreasing) effect on both GSH content and GSH/GSSG ratio supports a relatively weak interference of the TPP-conjugated peptides with cell redox status. According to LC–MS/MS analysis, the peptides generally cause some additive formation of GSSG (by up to 1.4 times), which was also observed for other antioxidants such as NAC (Zhang et al., 2011; Grosicka-Maciąg et al., 2011).

5. Conclusion

TPP cation can be regarded as a multi-functional moiety in cell-penetrating amphipathic cationic oligopeptides. Considering controversial data on TPP-mediated cellular delivery of peptide cargo, this study clarifies the role of TPP cation on pharmacokinetics-related properties of the oligopeptides. The TPP moiety further increases cellular uptake of YrFK peptide as well as its proteolytic stability, suggesting a way to improve cellular activity of the oligopeptides. However, the TPP-conjugated oligopeptides do not show the ability to disturb or readily penetrate across the mitochondrial inner membrane similarly as the unmodified oligopeptides. The evidence is provided that redox inactive TPP moiety is capable of increasing radical-scavenging and reducing activity of YrFK/YRFK in association with TPP-induced intramolecular interaction. Using model human cells, the TPP-conjugated peptides were shown to exhibit enhanced inhibitory effects against overproduced mitochondrial and cytoplasmic ROS without significant interfering with glutathione/redox status. Altogether, the results provide the basis of using the TPP modifier to improve both pharmacokinetic properties and specific activity of amphipathic cationic oligopeptides by targeting them to cellular ROS and increasing their stability and availability. Our study particularly identifies TPP3-YrFK as a promising cellular antioxidant, encouraging its further investigation.

Funding

The study was funded by the Russian Science Foundation according to the research project no.20-73-10105. The authors acknowledge the support of the subsidy allocated to Kazan Federal University for the state assignment in the sphere of scientific activities (project FZSM-2022-0020).

Data statement

The data presented in this study are contained within the article.

CRediT authorship contribution statement

Rezeda A. Ishkaeva: Investigation, Writing – original draft. **Diana V. Salakhieva:** Investigation. **Ruslan Garifullin:** Methodology, Investigation. **Raghad Alshadidi:** Investigation. **Alexander V. Laikov:** Methodology, Software. **Abdulla A. Yergeshov:** Formal analysis, Software. **Marat I. Kamalov:** Investigation. **Timur I. Abdullin:** Conceptualization, Supervision, Writing – review & editing.

Declaration of competing interest

The authors declare that they have no known competing financial interests or personal relationships that could have appeared to influence the work reported in this paper.

Data availability

Data will be made available on request.

Acknowledgement

The equipment of Interdisciplinary Centre for Shared Use of Kazan Federal University (KFU) was used. The authors thank Amina G. Daminova (Interdisciplinary Center for Analytical Microscopy of KFU) for LSCM analysis.

Appendix A. Supplementary data

Supplementary data to this article can be found online at https://doi.org/10.1016/j.crphar.2022.100148.

References

Abu-Gosh, S.E., Kolvazon, N., Tirosh, B., Ringel, I., Yavin, E., 2009. Multiple triphenylphosphonium cations shuttle a hydrophilic peptide into mitochondria. Mol. Pharm. 6 (4), 1138–1144. https://doi.org/10.1021/mp900032r.

Akasov, R., Zaytseva-Zotova, D., Burov, S., Leko, M., Dontenwill, M., Chiper, M., Vandamme, T., Markvicheva, E., 2016. Formation of multicellular tumor spheroids induced by cyclic RGD-peptides and use for anticancer drug testing *in vitro*. Int. J. Pharm. 506 (1–2), 148–157. https://doi.org/10.1016/j.ijpharm.2016.04.005.

Akhmadishina, R.A., Garifullin, R., Petrova, N.V., Kamalov, M.I., Abdullin, T.I., 2018. Triphenylphosphonium moiety modulates proteolytic stability and potentiates neuroprotective activity of antioxidant tetrapeptides *in vitro*. Front. Pharmacol. 9, 115. https://doi.org/10.3389/fphar.2018.00115.

Allen, M.E., Pennington, E.R., Perry, J.B., Dadoo, S., Makrecka-Kuka, M., Dambrova, M., Moukdar, F., Patel, H.D., Han, X., Kidd, G.K., Benson, E.K., Raisch, T.B., Poelzing, S., Brown, D.A., Shaikh, S.R., 2020. The cardiolipin-binding peptide elamipretide mitigates fragmentation of cristae networks following cardiac ischemia reperfusion in rats. Commun. Biol. 3 (1), 389. https://doi.org/10.1038/s42003-020-1101-3.

Alta, R.Y.P., Vitorino, H.A., Goswami, D., Teresa Machini, M., Esposito, B.P., 2017. Triphenylphosphonium-desferrioxamine as a candidate mitochondrial iron chelator. Biometals 30 (5), 709–718. https://doi.org/10.1007/s10534-017-0039-5.

Aon, M.A., Cortassa, S., Maack, C., O'Rourke, B., 2007. Sequential opening of mitochondrial ion channels as a function of glutathione redox thiol status. J. Biol. Chem. 282 (30), 21889–21900. https://doi.org/10.1074/jbc.M702841200.

Bielski, E.R., Zhong, Q., Brown, M., da Rocha, S.R., 2015. Effect of the conjugation density of triphenylphosphonium cation on the mitochondrial targeting of poly(amidoamine) dendrimers. Mol. Pharm. 12 (8), 3043–3053. https://doi.org/10.1021/acs.molpharmaceut.5b00320.

Cerrato, C.P., Pirisinu, M., Vlachos, E.N., Langel, U., 2015. Novel cell-penetrating peptide targeting mitochondria. Faseb. J. 29 (11), 4589–4599. https://doi.org/10.1096/fj.14-269225.

Chan, W., White, P., 1999. Fmoc Solid Phase Peptide Synthesis: A Practical Approach. Oxford University Press, Oxford. https://doi.org/10.1093/oso/9780199637256.001.0001.

Chavez, J.D., Tang, X., Campbell, M.D., Reyes, G., Kramer, P.A., Stuppard, R., Keller, A., Zhang, H., Rabinovitch, P.S., Marcinek, D.J., Bruce, J.E., 2020. Mitochondrial protein interaction landscape of SS-31. Proc. Natl. Acad. Sci. U.S.A. 117 (26), 15363–15373. https://doi.org/10.1073/pnas.2002250117.

Dai, D.F., Chen, T., Szeto, H., Nieves-Cintron, M., Kutyavin, V., Santana, L.F., Rabinovitch, P.S., 2011. Mitochondrial targeted antioxidant peptide ameliorates hypertensive cardiomyopathy. J. Am. Coll. Cardiol. 58 (1), 73–82. https://doi.org/10.1016/j.jacc.2010.12.044.

Escribano-Lopez, I., Diaz-Morales, N., Iannantuoni, F., Lopez-Domenech, S., de Maranon, A.M., Abad-Jimenez, Z., Banuls, C., Rovira-Llopis, S., Herance, J.R., Rocha, M., Victor, V.M., 2018. The mitochondrial antioxidant SS-31 increases SIRT1 levels and ameliorates inflammation, oxidative stress and leukocyte-endothelium interactions in type 2 diabetes. Sci. Rep. 8 (1), 15862. https://doi.org/10.1038/s41598-018-34251-8.

Firuzi, O., Miri, R., Tavakkoli, M., Saso, L., 2011. Antioxidant therapy: current status and future prospects. Curr. Med. Chem. 18 (25), 3871–3888. https://doi.org/10.2174/092986711803414368.

Fisher Scientific, T., 2017. The Molecular Probes Handbook. A Guide to Fluorescent Probes and Labeling Technologies. Generating and Detecting Reactive Oxygen Species. Thermo Fisher Scientific, Waltham, USA. Available online: https://www.thermofisher.com/ru/ru/home/references/molecular-probes-the-handbook/probes-for-reactive-oxygen-species-including-nitric-oxide/generating-and-detecting-reactive-oxygen-species.html.

Forman, H.J., Zhang, H., 2021. Targeting oxidative stress in disease: promise and limitations of antioxidant therapy. Nat. Rev. Drug Discov. 20 (9), 689–709. https://doi.org/10.1038/s41573-021-00233-1.

Garifullin, R., Blokhin, D.S., Akhmadishina, R.A., Petrova, N.V., Kusova, A.M., Klochkov, V.V., Abdullin, T.I., 2019. Effect of triphenylphosphonium moiety on spatial structure and biointeractions of stereochemical variants of YRFK motif. Eur. Biophys. J. 48 (1), 25–34. https://doi.org/10.1007/s00249-018-1327-x.

Gentilucci, L., De Marco, R., Cerisoli, L., 2010. Chemical modifications designed to improve peptide stability: incorporation of non-natural amino acids, pseudo-peptide bonds, and cyclization. Curr. Pharmaceut. Des. 16 (28), 3185–3203. https://doi.org/10.2174/138161210793292555.

Grosicka-Maciąg, E., Kurpios-Piec, D., Szumiło, M., Grzela, T., Rahden-Staroń, I., 2011. Protective effect of N-acetyl-L-cysteine against maneb induced oxidative and apoptotic injury in Chinese hamster V79 cells. Food Chem. Toxicol. 49 (4), 1020–1025. https://doi.org/10.1016/j.fct.2011.01.009.

Hong, T.H., Jeena, M.T., Kim, O.H., Kim, K.H., Choi, H.J., Lee, K.H., Hong, H.E., Ryu, J.H., Kim, S.J., 2021. Application of self-assembly peptides targeting the mitochondria as a novel treatment for sorafenib-resistant hepatocellular carcinoma cells. Sci. Rep. 11 (1), 874. https://doi.org/10.1038/s41598-020-79536-z.

Horton, K.L., Pereira, M.P., Stewart, K.M., Fonseca, S.B., Kelley, S.O., 2012. Tuning the activity of mitochondria-penetrating peptides for delivery or disruption. Chembiochem 13 (3), 476–485. https://doi.org/10.1002/cbic.201100415.

Horton, K.L., Stewart, K.M., Fonseca, S.B., Guo, Q., Kelley, S.O., 2008. Mitochondria-penetrating peptides. Chem. Biol. 15 (4), 375–382. https://doi.org/10.1016/j.chembiol.2008.03.015.

Huang, L., Yappert, M.C., Jumblatt, M.M., Borchman, D., 2008. Hyperoxia and thyroxine treatment and the relationships between reactive oxygen species generation, mitochondrial membrane potential, and cardiolipin in human lens epithelial cell cultures. Curr. Eye Res. 33 (7), 575–586. https://doi.org/10.1080/02713680802167554.

Ishkaeva, R.A., Nizamov, I.S., Blokhin, D.S., Urakova, E.A., Klochkov, V.V., Nizamov, I.D., Gareev, B.I., Salakhieva, D.V., Abdullin, T.I., 2021. Dithiophosphate-induced redox conversions of reduced and oxidized glutathione. Molecules 26 (10). https://doi.org/10.3390/molecules26102973.

Ishkaeva, R.A., Z, M., Laikov, A.V., Angelova, P.R., Abdullin, T.I., 2022. Probing cell redox state and glutathione-modulating factors using a monochlorobimane-based microplate assay. Antioxidants 11 (2), 391. https://doi.org/10.3390/antiox11020391.

Kim, D.J., Jeena, M.T., Kim, O.H., Hong, H.E., Seo, H., Ryu, J.H., Kim, S.J., 2020. Novel therapeutic application of self-assembly peptides targeting the mitochondria in *in vitro* and *in vivo* experimental models of gastric cancer. Int. J. Mol. Sci. 21 (17). https://doi.org/10.3390/ijms21176126.

Kolevzon, N., Kuflik, U., Shmuel, M., Benhamron, S., Ringel, I., Yavin, E., 2011. Multiple triphenylphosphonium cations as a platform for the delivery of a pro-apoptotic peptide. Pharm. Res. (N. Y.) 28 (11), 2780–2789. https://doi.org/10.1007/s11095-011-0494-6.

Le Gal, K., Ibrahim, M.X., Wiel, C., Sayin, V.I., Akula, M.K., Karlsson, C., Dalin, M.G., Akyürek, L.M., Lindahl, P., Nilsson, J., Bergo, M.O., 2015. Antioxidants can increase melanoma metastasis in mice. Sci. Transl. Med. 7 (308). https://doi.org/10.1126/scitranslmed.aad3740, 308re8-308re8.

Lucana, M.C., Arruga, Y., Petrachi, E., Roig, A., Lucchi, R., Oller-Salvia, B., 2021. Protease-resistant peptides for targeting and intracellular delivery of therapeutics. Pharmaceutics 13 (12), 2065. https://doi.org/10.3390/pharmaceutics13122065.

Manczak, M., Mao, P., Calkins, M.J., Cornea, A., Reddy, A.P., Murphy, M.P., Szeto, H.H., Park, B., Reddy, P.H., 2010. Mitochondria-targeted antioxidants protect against amyloid-beta toxicity in Alzheimer's disease neurons. J. Alzheim. Dis. 20 (2), S609–S631. https://doi.org/10.3233/JAD-2010-100564.

Meloni, B.P., Mastaglia, F.L., Knuckey, N.W., 2020. Cationic arginine-rich peptides (CARPs): a novel class of neuroprotective agents with a multimodal mechanism of action. Front. Neurol. 11, 108. https://doi.org/10.2174/0929866525666181101105209.

Mitchell, W., Ng, E.A., Tamucci, J.D., Boyd, K.J., Sathappa, M., Coscia, A., Pan, M., Han, X., Eddy, N.A., May, E.R., Szeto, H.H., Alder, N.N., 2020. The mitochondria-targeted peptide SS-31 binds lipid bilayers and modulates surface electrostatics as a key component of its mechanism of action. J. Biol. Chem. 295 (21), 7452–7469. https://doi.org/10.1074/jbc.RA119.012094.

Mizuguchi, Y., Chen, J., Seshan, S.V., Poppas, D.P., Szeto, H.H., Felsen, D., 2008. A novel cell-permeable antioxidant peptide decreases renal tubular apoptosis and damage in unilateral ureteral obstruction. Am. J. Physiol. Ren. Physiol. 295 (5), F1545–F1553. https://doi.org/10.1152/ajprenal.00395.2007.

Nag, L., Sournia, P., Myllykallio, H., Liebl, U., Vos, M.H., 2017. Identification of the TyrOH(*+) radical cation in the flavoenzyme TrmFO. J. Am. Chem. Soc. 139 (33), 11500–11505. https://doi.org/10.1021/jacs.7b04586.

Nazarov, P.A., Osterman, I.A., Tokarchuk, A.V., Karakozova, M.V., Korshunova, G.A., Lyamzaev, K.G., Skulachev, M.V., Kotova, E.A., Skulachev, V.P., Antonenko, Y.N., 2017. Mitochondria-targeted antioxidants as highly effective antibiotics. Sci. Rep. 7 (1), 1394. https://doi.org/10.1038/s41598-017-00802-8.

Powers, S.K., Hudson, M.B., Nelson, W.B., Talbert, E.E., Min, K., Szeto, H.H., Kavazis, A.N., Smuder, A.J., 2011. Mitochondria-targeted antioxidants protect against mechanical ventilation-induced diaphragm weakness. Crit. Care Med. 39 (7), 1749–1759. https://doi.org/10.1097/CCM.0b013e3182190b62.

Prasad, J., Machhi, H.K., Sonigara, K.K., Patel, V.K., Soni, S.S., 2020. Above 800 mV open-circuit voltage in solid-state photovoltaic devices using phosphonium cation-based solid ionic conductors. ACS Appl. Mater. Interfaces 12 (20), 22939–22947. https://doi.org/10.1021/acsami.0c04426.

Rocha, M., Hernandez-Mijares, A., Garcia-Malpartida, K., Banuls, C., Bellod, L., Victor, V.M., 2010. Mitochondria-targeted antioxidant peptides. Curr. Pharmaceut. Des. 16 (28), 3124–3131. https://doi.org/10.2174/138161210793292519.

Roelofs, B.A., Ge, S.X., Studlack, P.E., Polster, B.M., 2015. Low micromolar concentrations of the superoxide probe MitoSOX uncouple neural mitochondria and inhibit complex IV. Free Radic. Biol. Med. 86, 250–258. https://doi.org/10.1016/j.freeradbiomed.2015.05.032.

Ross, M.F., Filipovska, A., Smith, R.A., Gait, M.J., Murphy, M.P., 2004. Cell-penetrating peptides do not cross mitochondrial membranes even when conjugated to a lipophilic cation: evidence against direct passage through phospholipid bilayers. Biochem. J. 383 (Pt. 3), 457–468. https://doi.org/10.1042/BJ20041095.

Ross, M.F., Murphy, M.P., 2004. Cell-penetrating peptides are excluded from the mitochondrial matrix. Biochem. Soc. Trans. 32 (Pt 6), 1072–1074. https://doi.org/10.1042/BST0321072.

Sheu, S.S., Nauduri, D., Anders, M.W., 2006. Targeting antioxidants to mitochondria: a new therapeutic direction. Biochim. Biophys. Acta 1762 (2), 256–265. https://doi.org/10.1016/j.bbadis.2005.10.007.

Sun, Y., Zhan, A., Zhou, S., Kuang, X., Shen, H., Liu, H., Xu, Y., 2019. A novel mitochondria-targeting tetrapeptide for subcellular de livery of nanoparticles. Chin. Chem. Lett. 30 (7), 1435–1439. https://doi.org/10.1016/j.cclet.2019.05.001.

Szeto, H.H., 2006a. Mitochondria-targeted peptide antioxidants: novel neuroprotective agents. AAPS J. 8 (3), E521–E531. https://doi.org/10.1208/aapsj080362.

Szeto, H.H., 2006b. Cell-permeable, mitochondrial-targeted, peptide antioxidants. AAPS J. 8 (2), E277–E283. https://doi.org/10.1007/BF02854898.

Szeto, H.H., 2008. Mitochondria-targeted cytoprotective peptides for ischemia-reperfusion injury. Antioxidants Redox Signal. 10 (3), 601–619. https://doi.org/10.1089/ars.2007.1892.

Szeto, H.H., Schiller, P.W., Zhao, K., Luo, G., 2005. Fluorescent dyes alter intracellular targeting and function of cell-penetrating tetrapeptides. Faseb. J. 19 (1), 118–120. https://doi.org/10.1096/fj.04-1982fje.

Theodossiou, T.A., Sideratou, Z., Katsarou, M.E., Tsiourvas, D., 2013. Mitochondrial delivery of doxorubicin by triphenylphosphonium-functionalized hyperbranched nanocarriers results in rapid and severe cytotoxicity. Pharm. Res. (N. Y.) 30 (11), 2832–2842. https://doi.org/10.1007/s11095-013-1111-7.

Toyama, S., Shimoyama, N., Szeto, H.H., Schiller, P.W., Shimoyama, M., 2018. Protective effect of a mitochondria-targeted peptide against the development of chemotherapy-induced peripheral neuropathy in mice. ACS Chem. Neurosci. 9 (7), 1566–1571. https://doi.org/10.1021/acschemneuro.8b00013.

Tsepaeva, O.V., Nemtarev, A.V., Abdullin, T.I., Grigor'eva, L.R., Kuznetsova, E.V., Akhmadishina, R.A., Ziganshina, L.E., Cong, H.H., Mironov, V.F., 2017. Design, synthesis, and cancer cell growth inhibitory activity of triphenylphosphonium derivatives of the triterpenoid betulin. J. Nat. Prod. 80 (8), 2232–2239. https://doi.org/10.1021/acs.jnatprod.7b00105.

Tsepaeva, O.V., Nemtarev, A.V., Salikhova, T.I., Abdullin, T.I., Grigor Eva, L.R., Khozyainova, S.A., Mironov, V.F., 2020. Synthesis, anticancer, and antibacterial activity of betulinic and betulonic acid C-28-triphenylphosphonium conjugates with variable alkyl linker length. Anti Cancer Agents Med. Chem. 20 (3), 286–300. https://doi.org/10.2174/1871520619666191014153554.

Tsepaeva, O.V., Salikhova, T.I., Grigor'eva, L.R., Ponomaryov, D.V., Dang, T., Ishkaeva, R.A., Abdullin, T.I., Nemtarev, A.V., Mironov, V.F., 2021. Synthesis and *in vitro* evaluation of triphenylphosphonium derivatives of acetylsalicylic and salicylic acids: structure-dependent interactions with cancer cells, bacteria, and mitochondria. Med. Chem. Res. 30 (4), 925–939. https://doi.org/10.1007/s00044-020-02674-6.

Vassalle, C., Maltinti, M., Sabatino, L., 2020. Targeting oxidative stress for disease prevention and therapy: where do we stand, and where do we go from here. Molecules 25 (11), 2653. https://doi.org/10.3390/molecules25112653.

Wang, J.Y., Li, J.Q., Xiao, Y.M., Fu, B., Qin, Z.H., 2020. Triphenylphosphonium (TPP)-based antioxidants: a new perspective on antioxidant design. ChemMedChem 15 (5), 404–410. https://doi.org/10.1002/cmdc.201900695.

Wang, X., Liu, J., Chen, J., Zhang, M., Tian, C., Peng, X., Li, G., Chang, W., Lou, H., 2021. Azole-triphenylphosphonium conjugates combat antifungal resistance and alleviate the development of drug-resistance. Bioorg. Chem. 110, 104771. https://doi.org/10.1016/j.bioorg.2021.104771.

Yang, B., Wang, T.-t., Yang, Y.-s., Zhu, H.-l., Li, J.-h., 2021. The application progress of peptides in drug delivery systems in the past decade. J. Drug Deliv. Sci. Technol. 66, 102880. https://doi.org/10.1016/j.jddst.2021.102880.

Yang, N.J., Hinner, M.J., 2015. Getting across the cell membrane: an overview for small molecules, peptides, and proteins. Methods Mol. Biol. 29–53. https://doi.org/10.1007/978-1-4939-2272-7_3.

Zhang, H., Limphong, P., Pieper, J., Liu, Q., Rodesch, C.K., Christians, E., Benjamin, I.J., 2011. Glutathione-dependent reductive stress triggers mitochondrial oxidation and cytotoxicity. Faseb. J. 26 (4), 1442–1451. https://doi.org/10.1096/fj.11-199869.

Zhang, Y., Wu, C., Guo, S., Zhang, J., 2013. Interactions of graphene and graphene oxide with proteins and peptides. Nanotechnol. Rev. 2 (1), 27–45. https://doi.org/10.1515/ntrev-2012-0078.

Zhao, K., Luo, G., Giannelli, S., Szeto, H.H., 2005. Mitochondria-targeted peptide prevents mitochondrial depolarization and apoptosis induced by tert-butyl hydroperoxide in neuronal cell lines. Biochem. Pharmacol. 70 (12), 1796–1806. https://doi.org/10.1016/j.bcp.2005.08.022.

Zhao, K., Luo, G., Zhao, G.M., Schiller, P.W., Szeto, H.H., 2003. Transcellular transport of a highly polar 3+ net charge opioid tetrapeptide. J. Pharmacol. Exp. Therapeut. 304 (1), 425–432. https://doi.org/10.1124/jpet.102.040147.

Zielonka, J., Joseph, J., Sikora, A., Hardy, M., Ouari, O., Vasquez-Vivar, J., Cheng, G., Lopez, M., Kalyanaraman, B., 2017. Mitochondria-targeted triphenylphosphonium-based compounds: syntheses, mechanisms of action, and therapeutic and diagnostic applications. Chem. Rev. 117 (15), 10043–10120. https://doi.org/10.1021/acs.chemrev.7b00042.